

# Sequence dependent aggregation of peptides and fibril formation

Nguyen Ba Hung,<sup>1,2,3</sup> Duy-Manh Le,<sup>1</sup> and Trinh X. Hoang<sup>1,2, a)</sup>

<sup>1)</sup>*Institute of Physics, Vietnam Academy of Science and Technology, 10 Dao Tan, Ba Dinh, Ha Noi, Viet Nam*

<sup>2)</sup>*Graduate University of Science and Technology, Vietnam Academy of Science and Technology, 18 Hoang Quoc Viet, Cau Giay, Ha Noi, Viet Nam*

<sup>3)</sup>*Vietnam Military Medical University, 160 Phung Hung, Ha Dong, Ha Noi, Viet Nam*

(Dated: 7 March 2019)

Deciphering the links between amino acid sequence and amyloid fibril formation is key for understanding protein misfolding diseases. Here we use Monte Carlo simulations to study aggregation of short peptides in a coarse-grained model with hydrophobic-polar (HP) amino acid sequences and correlated side chain orientations for hydrophobic contacts. A significant heterogeneity is observed in the aggregate structures and in the thermodynamics of aggregation for systems of different HP sequences and different number of peptides. Fibril-like ordered aggregates are found for several sequences that contain the common HPH pattern while other sequences may form helix bundles or disordered aggregates. A wide variation of the aggregation transition temperatures among sequences, even among those of the same hydrophobic fraction, indicates that not all sequences undergo aggregation at a presumable physiological temperature. The transition is found to be the most cooperative and first-order like for sequences forming fibril-like structures. For a fibril-prone sequence, it is shown that fibril formation follows the nucleation and growth mechanism. Interestingly, a binary mixture of peptides of an aggregation-prone and a non-aggregation-prone sequence shows association and conversion of the latter to the fibrillar structure. Our study highlights the role of sequence in selecting fibril-like aggregates and also the impact of structural template on fibril formation by peptides of unrelated sequences.

## I. INTRODUCTION

The phenomenon in which soluble proteins or protein fragments self-assemble into insoluble aggregates is considered as a fundamental issue of protein folding with serious impact on human health<sup>1</sup>. A predominant class of these aggregates, that have a long straight shape and are rich in  $\beta$ -sheets, known as amyloid fibrils, is associated to a range of debilitating human pathologies, such as Alzheimer's, Parkinson's, type II diabetes and transmissible spongiform encephalopathies<sup>2</sup>. These fibrils, formed by numerous proteins and peptides including those unrelated to disease<sup>3</sup>, have strikingly similar structural features regardless of the amino acid sequence. An widely adopted view is that the tendency of forming amyloid fibrils is a common property of all proteins, supposedly due to their common polypeptide backbone<sup>4</sup>. It has been shown that poly-aminoacids can also form amyloid under appropriate condition<sup>5</sup>. However, the propensity of a given polypeptide to form amyloid fibrils as well as the condition under which they form depends very significantly on its amino acid sequence showing that the problem is much more complex than it could be initially thought of but also giving hope for curing amyloid diseases<sup>6</sup>.

X-ray fiber diffraction data indicate that amyloid fibrils are commonly characterized by the cross- $\beta$ -sheets with strands running perpendicularly to the fibril's lon-

gitudinal axis<sup>7</sup>. The cross- $\beta$ -structures at atomic resolution have been obtained for the fibrils of a few proteins and peptides including insulin<sup>8</sup>,  $\beta$ -amyloid peptide<sup>9</sup>, HET-s prion<sup>10</sup>, and  $\alpha$ -synuclein<sup>11</sup> by using cryo-electron microscopy, X-ray and solid-state NMR. It is found that they are highly ordered and composed of  $\beta$ -strands of the same segments of repetitive protein molecules. Between the mated  $\beta$ -sheets is a complete dry and complementary packing of amino acid side chains with a well-formed hydrophobic core<sup>12</sup>. Even though there are evidence of polymorphism<sup>13</sup> in amyloid fibrils, the observed packing of side chains in the resolved structures has suggested that the amino acid sequence dictates much the amyloid fold<sup>14</sup>, in the same manner as in protein folding.

The sequence determinant of amyloid formation has been studied with various experimental<sup>15–21</sup> and theoretical<sup>22,23</sup> approaches. It has been shown that the overall hydrophobicity<sup>17</sup> and net charge<sup>19</sup> of a peptide, to some extent, may impact the aggregation rate. There are increasing evidence that the capability of a protein to form amyloids strongly depends on certain short amino acid stretches in the sequence<sup>16–18</sup>. To support a proteome-wide search for aggregation-prone peptide segments, a number of predictors have been made available<sup>24–26</sup>. However, the problem still substantially needs better understanding.

In this study, we investigate the selectivity of aggregate structures by the amino acid sequence and the mechanism of fibril formation by using the tube model of protein<sup>27</sup>. The tube model is a fully backbone-based model that exploits the tube-like symmetry of a polypeptide chain<sup>28</sup> and the geometrical constraints imposed by

<sup>a)</sup> Electronic mail: [hoang@iop.vast.vn](mailto:hoang@iop.vast.vn)

hydrogen bonds<sup>29</sup>. Such a model has been shown to form protein-like low energy structures<sup>27</sup> as well as amyloid-like aggregates<sup>29,30</sup>. A variant of the tube model has been used to study the aggregation for homopolymeric peptide<sup>31,32</sup>. In the present study, we focus on the impact of amino acid sequence on the aggregation properties with a renewed consideration of hydrophobic interaction. In the original tube model, the latter was based on an isotropic contact potential between centroids represented by the  $C_\alpha$  atoms. We introduce here a new model for hydrophobic contact between amino acids that takes into account the side chain orientations. We find that the latter can direct the interaction between  $\beta$ -sheets and promote the formation of ordered and elongated fibril-like aggregates.

We restrict ourself to hydrophobic-polar (HP) sequences and short peptides of length equal to 8 residues. The consideration of HP sequences is a minimalist approach in terms of sequence specificity, however is well supported in protein folding<sup>30,33</sup>. Furthermore, the rather simplicity of amyloid fibril structures also indicates a possible simplification of the amino acid sequence in determining aggregation properties. It will be shown that even with a short length and a few sequences, the systems considered already exhibit a rich behavior in the morphologies of the aggregates and in their thermodynamic properties.

For an aggregation-prone sequence, we have studied also the kinetics of fibril formation. We will try to elucidate the nucleation and growth mechanism of this process at molecular detail and show evidence of a lag phase. Finally, we have studied a binary mixture of peptides of two different sequences and find that amyloid formation can be sequence non-specific, that is a fibril-like template formed by an aggregation-prone sequence may induce aggregation of a non-aggregation-prone sequence for a fraction of all peptides. This strong impact of the template decreases somewhat the sequence determination of aggregation propensity and suggests that amyloid fibrils could be heterogeneous in their peptide composition.

## II. MODELS AND METHODS

Details of the tube model can be found in Ref.<sup>27</sup>. Briefly, it is a  $C_\alpha$ -based coarse-grained model, in which the  $C_\alpha$  atoms representing amino acid residues are placed along the axis of a self-avoiding tube of cross-sectional radius  $\Delta = 2.5\text{\AA}$ . The finite thickness of the tube is imposed by requiring the radius of circle drawn through any three  $C_\alpha$  atoms must be larger than  $\Delta$ <sup>28,34</sup>. The energy of a given conformation is the sum of the bending energy, hydrogen bonding energy and hydrophobic interaction energy. A local bending energy penalty of  $e_R = 0.3\epsilon > 0$ , with  $\epsilon$  an energy unit, is applied if the chain local radius of curvature at a given bead is less than  $3.2\text{\AA}$ . Hydrogen bonds between amino acids are required to satisfy a set of distance and angular constraints on the

local properties of the chain as found by a statistical analysis of protein PDB structures<sup>29</sup>. Local hydrogen bond, which is formed by residues separated by three peptide bonds along the chain, is given an energy of  $-\epsilon$ , whereas non-local hydrogen bond is given an energy of  $-0.7\epsilon$ . Additionally, a cooperative energy of  $-0.3\epsilon$  is given for each pair of hydrogen bonds that are formed by pairs of consecutive amino acids in the sequence. To avoid spurious effects of the chain termini, hydrogen bonds involving a terminal residue are given a reduced energy of  $-0.5\epsilon$ .

Hydrophobic interaction is based on the pairwise contacts between amino acids, considered to be either hydrophobic (H) or polar (P). It is also assumed that only contacts between H residues are favorable, and thus the contact energies of different residues pairing are  $e_{HH} = -0.5\epsilon$ , and  $e_{HP} = e_{PP} = 0$ . In the original tube model, a contact is defined if the distance between two residues is less than  $7.5\text{\AA}$ . In the present study, we apply an additional constraint on hydrophobic contact by taking into account the side chain orientation<sup>35</sup> (Fig. 1a,b). The latter are approximately given by the inverse direction to the normal vector<sup>36</sup> at the chain's local position. The new constraint requires that two residues  $i$  and  $j$  make a hydrophobic contact if  $\mathbf{n}_i \cdot \mathbf{c}_{ij} < 0.5$  and  $\mathbf{n}_j \cdot \mathbf{c}_{ji} < 0.5$  where  $\mathbf{n}_i$  and  $\mathbf{n}_j$  are the normal vectors of the Frenet frames associated with bead  $i$  and  $j$ , respectively;  $\mathbf{c}_{ij}$  is an unit vector pointing from bead  $i$  to bead  $j$ ; and  $\mathbf{c}_{ji} = -\mathbf{c}_{ij}$ . These vectors are given by

$$\mathbf{n}_i = \frac{\mathbf{r}_{i-1} + \mathbf{r}_{i+1} - 2\mathbf{r}_i}{|\mathbf{r}_{i-1} + \mathbf{r}_{i+1} - 2\mathbf{r}_i|}, \quad (1)$$

and

$$\mathbf{c}_{ij} = \frac{\mathbf{r}_j - \mathbf{r}_i}{|\mathbf{r}_j - \mathbf{r}_i|}, \quad (2)$$

where  $\mathbf{r}_i$  is the position of bead  $i$ . The new constraint is in accordance with the statistics drawn from an analysis of PDB structures (Fig. 1b).

Monte Carlo (MC) simulations are carried out for systems of  $M$  peptides in a cubic box of size  $L$  with periodic boundary conditions. Parallel tempering<sup>37</sup> Monte Carlo schemes with 16-24 replicas at different temperatures are employed for obtaining the system ground state and equilibrium characteristics. For each replica, the simulation is carried out with pivot, crankshaft and translation moves and with the Metropolis algorithm for move acceptance at its own temperature  $T_i$ . A replica exchange attempt is made every 10 MC sweeps (one sweep corresponds to a number of move attempts equal to the number of residues). The exchange of replicas  $i$  and  $j$  is accepted with a probability  $p = \min\{1, \exp[(\beta_i - \beta_j)(E_i - E_j)]\}$ , where  $\beta = (k_B T)^{-1}$  is the inverse temperature,  $k_B$  is the Boltzmann constant, and  $E_i$  and  $E_j$  are the energies of the replicas at the time of the exchange.

The temperature range in parallel tempering simulations are chosen such that it covers the transition from a gas phase of separated peptides at a high temperature to the condensed phase of the aggregates at a low

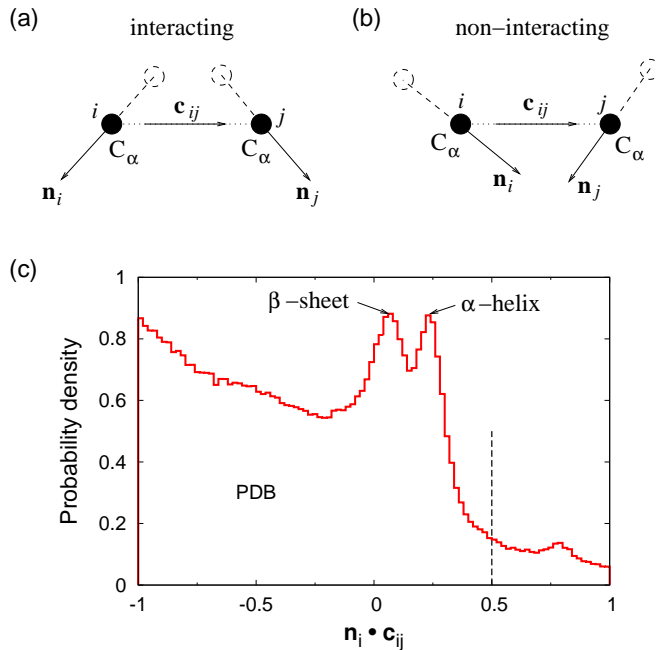


FIG. 1. (a and b) Model of contact interaction with correlated side chain orientations. The side chains are assumed to be placed in the inverse direction to the normal vectors,  $\mathbf{n}_i$  and  $\mathbf{n}_j$ , from the  $C_\alpha$  atoms. Two amino acids interact if their side chains are oriented towards each other (a), or do not interact if the side chains are oriented apart from each other (b). (c) Histogram of the product  $\mathbf{n}_i \cdot \mathbf{c}_{ij}$  for side chain - side chain contacts obtained from 500 filtered PDB structures of the top500 database. The latter contacts are defined if there are at least two atoms, separately belonged to the two side chains, found at a distance less than 1.5 times the sum of their van der Waals radii. The peaks near the center of the histogram correspond to the contributions of  $\alpha$ -helices and  $\beta$ -sheets as indicated. Vertical dash line indicates the cut-off used in the model.

temperature. The replica temperatures are chosen such that acceptance rates of replica exchanges for neighboring temperatures are significant, of at least about 20%. Practically, one needs to change the set of temperatures several times in such a way that there are more temperatures near the specific heat's peak, where the energy fluctuation is large. The number of Monte Carlo attempted moves is of the order of  $10^9$  per replica. The weighted multiple histogram technique<sup>38</sup> is employed for the calculation of equilibrium properties such as the specific heat and the effective free energy.

For studying the kinetics of fibril growth, we carry out multiple independent Monte Carlo simulations that start from random configurations of dispersed monomers. These initial configurations are equilibrated at a high temperature before being used. We are interested in three quantities: the number of aggregates, the maximum size of the aggregates, and the number of peptides in  $\beta$ -sheet conformation during the time evolution. A

TABLE I. HP sequences of amino acids of peptides considered in present study (H – hydrophobic, P – polar). The parameter  $s$  denotes the minimal sequence separation between two consecutive H amino acids.

Sequence name	Sequence	$s$
S1	P P P H H P P P	1
S2	P P H P H P P P	2
S3	P P H P P H P P	3
S4	P H P P P H P P	4
S5	P H P P P P H P	5
S6	H P P P P P H P	6
S7	H P P P P P P H	7
S8	P P H H H P P P	1
S9	P P H P H H P P	1
S10	P H P P H H P P	1
S11	P H P H P H P P	2
S12	P H P P H P H P	2

peptide is said to be in a  $\beta$ -sheet conformation if it forms at least 4 consecutive hydrogen bonds with another peptide.

We will consider 12 HP sequences of length  $N = 8$  as given in Table I. The sequences, denoted as S1 through S12, are selected in such a way that they contain only 2 or 3 H residues, corresponding to hydrophobic fraction of 25% and 37.5%, respectively. We consider only sequences that are symmetric as much as possible from the two ends having in mind that the relative positions of the H residues are more important than their absolute positions in the sequence. One characterization of these relative positions is the minimum separation between two consecutive H residues given by the parameter  $s$  in Table I. The number of chains  $M$  considered is varied up to 20. The box size  $L$  is chosen depending on  $M$  and the peptide concentration  $c$ . For example, for  $M = 10$  and  $c = 1$  mM one gets  $L = 255.15\text{\AA}$ .

### III. RESULTS

#### A. Sequence dependence of aggregate structures

We first study the dependence of aggregate structure on the amino acid sequence for systems of  $M = 10$  identical peptides at a fixed concentration of 1 mM. Fig. 2 shows that the lowest energy conformation obtained in the simulations, supposed to be the ground state of a given system, strongly depends on the sequence. Two sequences, S2 and S11, form a double layer  $\beta$ -sheet structure with characteristics similar to that of a cross- $\beta$  structure. In these structures, an axis of the aggregate approximately perpendicular to the  $\beta$ -strands can be drawn. A similar structure but less fibril-like is also found for sequence S12 with some parts that are non- $\beta$ -sheet. Both

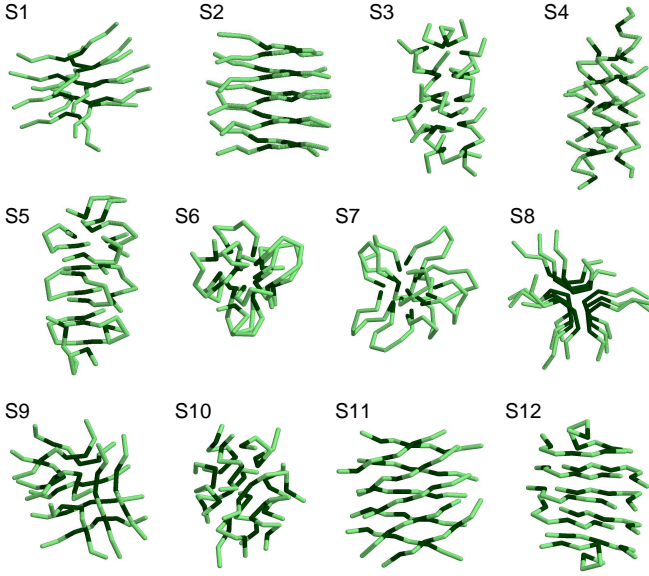


FIG. 2. Ground state conformations obtained by the simulations for systems of  $M = 10$  peptides for 10 HP sequences (S1–S10) as given in Table I. The hydrophobic (polar) residues are shown in dark (light) green color.

sequences S3 and S4 form a  $\alpha$ -helix bundle. The helix bundle of sequence S4 however is more ordered and has an approximate cylinder shape, in which the  $\alpha$ -helices are almost parallel to each other. This type of aggregate is akin to non-amyloid filaments formed by globular proteins such as the actin filament<sup>39</sup>. Other sequences form some sorts of disordered aggregates. In these disordered structures one may also find a significant fraction of  $\beta$ -sheets.

The role of hydrophobic residues in aggregation can be figured out from the structures of the aggregates. In all cases, one finds the presence of a well-formed hydrophobic core with the putative hydrophobic side chains oriented inwards to the body of the aggregate. The packing of hydrophobic side chains is best observed for sequences S2 and S11, for which the hydrophobic residues are aligned within each  $\beta$ -sheet and the hydrophobic side chains from the two  $\beta$ -sheets are facing each other. This packing is possible due to the HPH pattern in these sequences which position the hydrophobic side chains on one side of each  $\beta$ -sheet. An alignment of hydrophobic residues is also seen for sequence S12 due to the HPH segment of this sequence. In the aggregate of sequences S4, which is a helix bundle, the hydrophobic side chains are gathered along the bundle axis, thanks to the alignment of hydrophobic side chains along one side of each  $\alpha$ -helix. This alignment is due to the HPPPH pattern in the S4 sequence. On the other hand, the S3 sequence with the HPPH pattern also forms a helix but the hydrophobic side chains are not well aligned in the helix, leading to a less ordered aggregate.

The structure of the aggregate also depends on the number of chains  $M$ . In Fig. 3 and Fig. 4, the ground

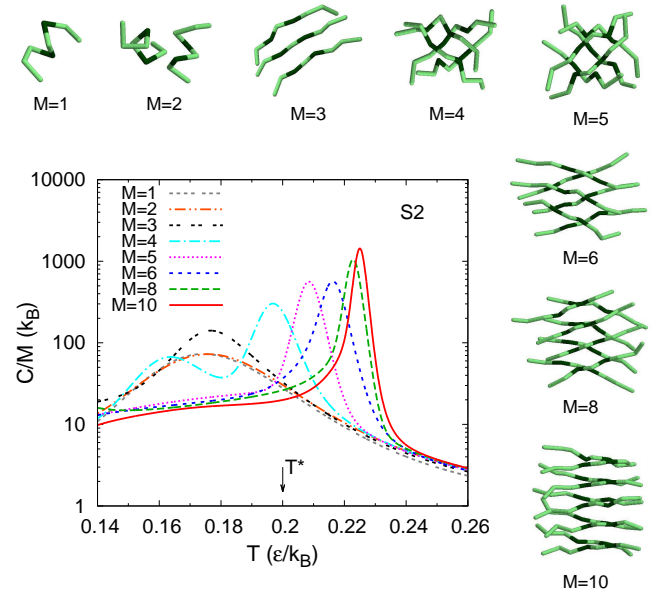


FIG. 3. Temperature dependence of the specific heat  $C$  per molecule for sequence S2 systems with the number of chains  $M$  equal to 1, 2, 3, 4, 5, 6, 8 and 10 as indicated. The conformations shown are ground state conformations obtained by the simulations for the systems considered. The position of a putative physiological temperature,  $T^*$ , is indicated.

states for  $M$  varying between 1 and 10 are shown for sequence S2 and S4, respectively. Interestingly, for sequence S2 (Fig. 3) as  $M$  increases one sees transitions from single helix to two-helix bundle, then to single  $\beta$ -sheet ( $M = 3$ ) and to double  $\beta$ -sheets ( $M \geq 4$ ). One can also notice that as  $M$  increases the  $\beta$ -sheet aggregates become more ordered and more fibril-like as their  $\beta$ -strands become more parallel. For sequences S4 (Fig. 4), only helix bundles are formed for all  $M > 1$ , but the bundle also becomes more ordered as  $M$  increases. Thus, the increasing orderliness with the system size is observed for both  $\beta$ -sheet and  $\alpha$ -helical aggregates.

## B. Thermodynamics of aggregation

It can be expected that the thermodynamics of aggregation depend on the aggregate structure due to distinct contributions of intermolecular and intramolecular interactions in different structures. Furthermore, the formations of ordered and non-ordered aggregates can be different from the perspective of a phase transition. We will consider the system's specific heat,  $C$ , for the analysis of the thermodynamics. We are particularly interested in the temperature of the main peak of the specific heat,  $T_{\text{peak}}$ , which corresponds to the aggregation transition, and the peak height,  $C_{\text{peak}}$ , which is a measure of the transition cooperativity. A sharp peak suggests that the transition is cooperative and first-order-like. On the other hand, a broad peak suggests a non-cooperative



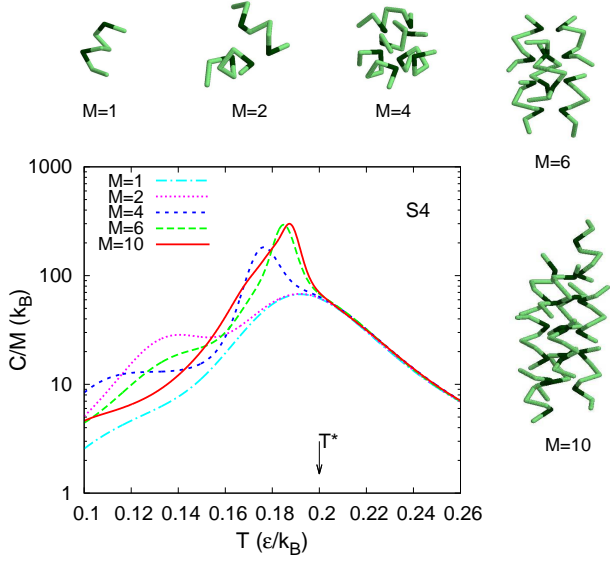


FIG. 4. Same as Fig. 3 but for sequence S4 systems. For clarity, the system sizes shown are fewer than for sequences S2.

transition which can be second-order-like.

We find that the specific heat strongly depends on both the sequence and the system size. Fig. 3 and Fig. 4 show the temperature dependence of the specific heat per molecule for various system sizes for sequences S2 and S4, respectively. For sequence S2, the case in which fibril-like aggregates form, it is shown that as  $M$  increases the specific heat's peak shifts toward higher temperature and its height increases (Fig. 3). This result indicates that the aggregate becomes increasingly stable and the transition becomes more cooperative as the system size increases. The increasing cooperativeness of the aggregation transition correlates with the increasing orderliness in the structure of the aggregate. For sequence S4, for which the aggregates are helix bundles, the height of the main peak increases with  $M$  but the position of the peak varies non-monotonically (Fig. 4). Note that the aggregation transition for sequences S4 is always found at a slightly lower temperature than the folding transition of individual chain. This is in contrast with sequence S2, whose aggregation transition temperature is always higher than the folding temperature of a single chain.

In Fig. 5, the results of the maximum specific heat per molecule,  $C_{\text{peak}}/M$ , and the temperature of the peak,  $T_{\text{peak}}$ , are combined for all sequences considered and for several values of  $M$ . It is shown that the variation of both  $C_{\text{peak}}/M$  and  $T_{\text{peak}}$  increases with  $M$ . Note that for  $M = 10$ , the highest specific heat maxima correspond to sequences S2 and S11 whose aggregates are fibril-like (see Fig. 2). Also for these two sequences,  $C_{\text{peak}}/M$  increases with  $M$  much faster than other sequences. Thus, the propensity of forming fibril-like aggregates can be linked to the cooperativity of the aggregation transition.

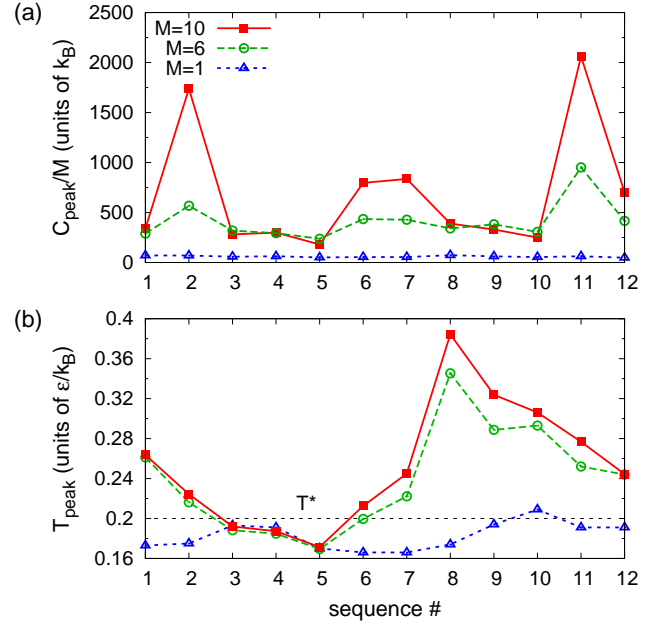


FIG. 5. Dependence of the maximum of the specific heat  $C_{\text{peak}}$  per molecule (a) and its temperature  $T_{\text{peak}}$  (b) on the sequence for systems of  $M = 10$  (solid),  $M = 6$  (dashed) and  $M = 1$  (dotted) peptides. The sequence number is given in accordance to Table I. The horizontal line in (b) indicates a putative physiological temperature  $T^*$ .

The wide variation in the transition temperatures  $T_{\text{peak}}$  among sequences, as shown in Fig. 5b, suggests another interesting aspect of aggregation. Suppose that we consider the systems at the physiological temperature,  $T^*$ . In our model, a rough estimate of  $T^*$  could be  $0.2 \epsilon/k_B$ , which corresponds to a local hydrogen bond energy of  $5 k_B T^*$ . For  $M = 1$ , one finds that all sequences but S10 has  $T_{\text{peak}} < T^*$  suggesting that the peptides are substantially unstructured at  $T^*$  as a single chain. For  $M = 6$  and  $M = 10$ , only three sequences, S3, S4 and S5, have  $T_{\text{peak}} < T^*$ , while the other have  $T_{\text{peak}} > T^*$ . Thus, sequences S3, S4 and S5 do not aggregate at  $T^*$  while other sequences do. This result indicates that the variation of aggregation transition temperatures among sequences is also a reason why protein sequences behave differently towards aggregation at the physiological temperature. Some sequences do not aggregate because aggregation is thermodynamically unfavorable at this temperature.

Note that the ability of forming fibril-like aggregates is not necessarily associated with a high aggregation transition temperature. In fact, Fig. 5b shows that sequences S2 and S11 have only a medium value of  $T_{\text{peak}}$  among all sequences, for both  $M = 6$  and  $M = 10$ . Some sequences with a higher  $T_{\text{peak}}$ , such as S8, S9 and S10, form disordered aggregates.

The dependence of specific heat on the system size also reveals a condition for aggregation. Fig. 3 shows that for sequence S2, systems of  $M \leq 4$  have the specific heat

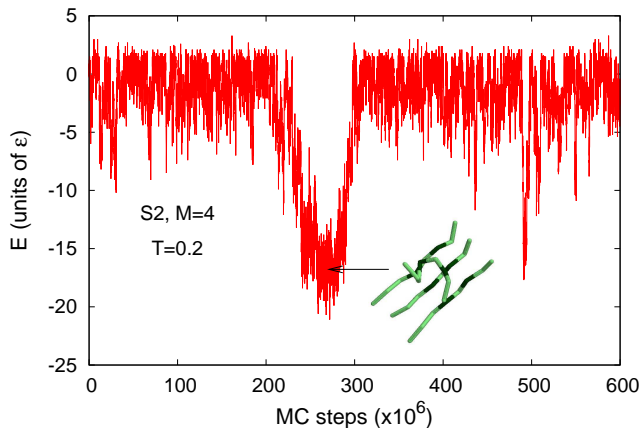


FIG. 6. Energy as function of Monte Carlo steps in a trajectory at  $T = 0.2$  for the sequence S2 system with  $M = 4$ . The conformation shown is a metastable state with a 3-peptide  $\beta$ -sheet in contact with a disordered helix formed by the 4th peptide.

peaked at a lower temperature than  $T^* = 0.2\epsilon/k_B$ , which means that these systems do not aggregate at  $T^*$ . Only for  $M > 4$ , the specific heat peak temperature is higher than  $T^*$  indicating that the fibril-like aggregates formed by this sequence are stable at  $T^*$ . Thus, a sufficient number of peptides is needed for the aggregation to happen at a given temperature. We also find that the lower peak in the specific heat of the system of  $M = 4$  (Fig. 3) corresponds to a transition from metastable aggregates at intermediate temperature to the ground state at low temperature. Fig. 6 shows the trajectory of an equilibrium simulation at  $T = 0.2\epsilon/k_B$  for sequences S2 with  $M = 4$ . The time dependence of the system's energy in this trajectory indicates that the peptides do not aggregate most of the time, so that the energy is relatively high, but for some short periods they can spontaneously form a metastable aggregate of a much lower energy. This metastable aggregate has a three-stranded  $\beta$ -sheet (Fig. 6, inset) and could act as a template for fibril growth in systems of more peptides.

### C. Kinetics of fibril formation

It is well-established that amyloid fibril formation follows the nucleation-growth mechanism, like in crystal and polymer growths<sup>40</sup>. The time dependence of fibril mass is characterized by an initial lag phase, during which the growth rate is small, before a period of rapid growth<sup>41–43</sup>. Nucleation gives rise to the lag phase and is a rate-limiting step. Simulations have suggested that primary nucleation events correspond to the formation of a fibril-like aggregate from disordered assemblies of molecules<sup>32</sup> and may involve metastable amyloid-like oligomers<sup>44</sup>. Experimental data indicate that amyloid

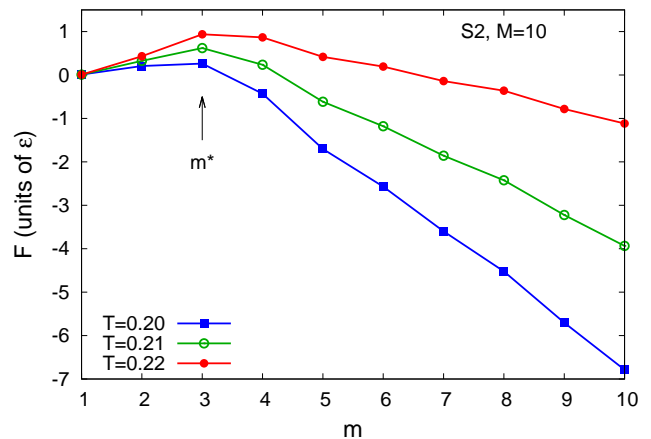


FIG. 7. Dependence of total free energy,  $F$ , on the size of the largest aggregate,  $m$ , for the sequence S2 system of  $M = 10$  peptides at three different temperatures,  $T = 0.2, 0.21$  and  $0.22 \epsilon/k_B$ , as indicated. The free energy of non-aggregated state, of  $m = 1$ , is used as reference. A barrier with the maximum located at  $m = 3$  is indicated.

fibril growth can be dominated by secondary nucleation events such as fragmentation<sup>43</sup> and surface-catalyzed nucleation<sup>45</sup>. In the following, we will investigate the behavior of fibril growth within our simple model for sequence S2.

First, we consider a system of  $M = 10$  peptides with concentration  $c = 1$  mM under equilibrium condition. Fig. 7 shows the dependence of the total free energy of the system on the size of the largest aggregate,  $m$ , formed at three temperatures slightly below  $T_{\text{peak}}$  including  $T = T^* = 0.2\epsilon/k_B$ . It is shown that for all these temperatures the free energy has a maximum at  $m = 3$ , suggesting that  $m = 3$  could be the size of the critical nucleus for fibril formation. Interestingly,  $M = 3$  is also the system size at which the ground state changes from a helix bundle to a  $\beta$ -sheet on increasing  $M$ , and this  $\beta$ -sheet is unstable at temperatures larger or equal  $T^*$  (see Fig. 3). Thus, there is a consistency between the equilibrium data obtained with a small and a larger  $M$  in terms of aggregation properties. The free energy barrier for aggregation in Fig. 7 is found to increase with  $T$  and is about of  $1 kT$  to  $4 kT$ . This barrier is not large and is consistent with the fact that the sequence considered is highly aggregation-prone. For  $m > 3$ , Fig. 7 shows that the free energy decreases almost linearly with  $n$ , which is consistent with the fact that the growth of the aggregate in size is essentially one-dimensional. After a certain size, new peptides join an existing aggregate from either of its two ends and establish the elongation of the  $\beta$ -sheets.

We then considered a larger system of  $M = 20$  peptides and studied the time evolutions from random configurations of dispersed monomers. Up to 100 independent trajectories are carried out to determine the statistics. We first consider the system at concentration  $c = 1$  mM and  $T = 0.2\epsilon/k_B$ . Fig. 8 (a and b) shows three typi-

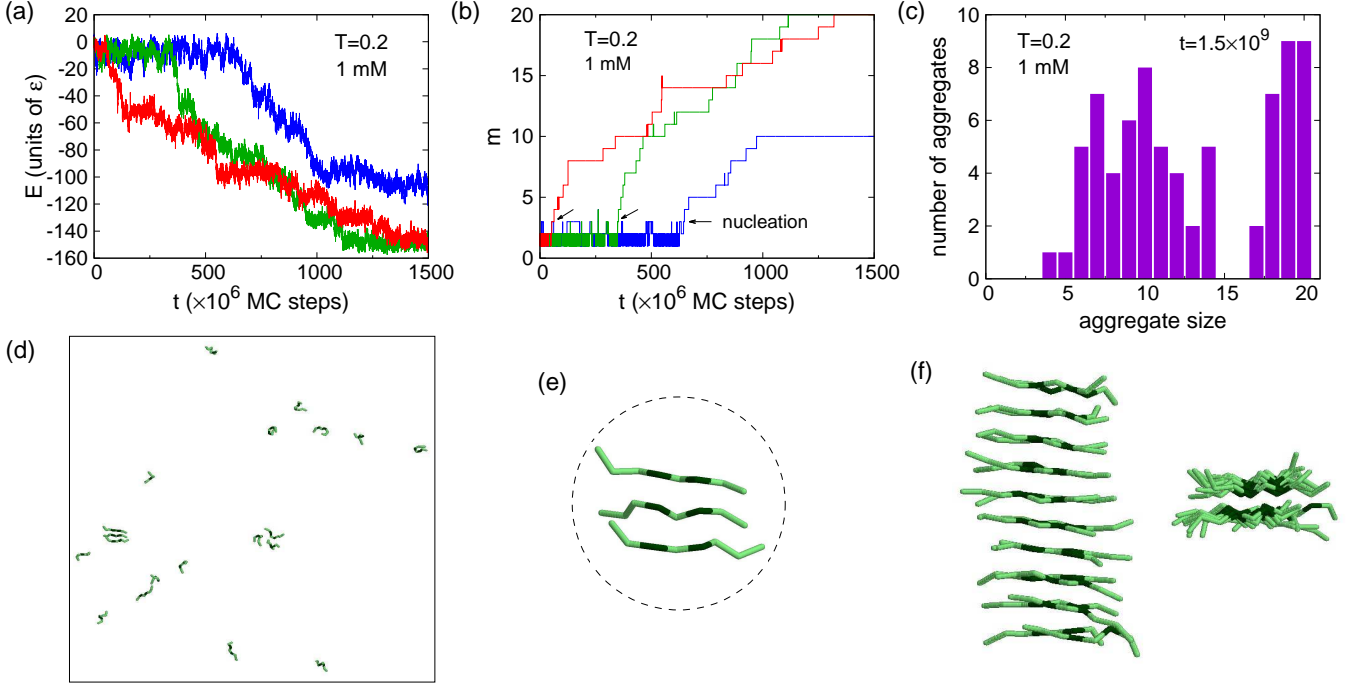


FIG. 8. Kinetics of fibril formation for sequence S2 with  $M = 20$  peptides at concentration  $1$  mM and temperature  $T = 0.2\epsilon/k_B$ . (a) Dependence of the energy,  $E$ , on time,  $t$ , measured in MC steps for three different trajectories. (b) Time dependence of the maximum aggregate size  $m$  for the same three trajectories as shown in (a). Arrows indicate nucleation event for each trajectory. (c) Histogram of the aggregate size given by the number of peptides obtained at a large time of  $t = 1.5 \times 10^9$  MC steps. (d) Snapshot of peptide configuration at a nucleation event. (e) Conformation of the nucleated cluster formed by three peptides taken from the configuration shown in (d). (f) Conformation of an elongated fibril-like structure formed by 20 peptides.

cal trajectories with the total energy  $E$  and the size of the largest aggregate  $m$  as functions of time. Interestingly, these trajectories show clear evidence of an initial lag time, during which  $m$  fluctuates but remains small ( $m \leq 3$ ) before a rapid and almost monotonic growth (Fig. 8 b). They also show that nucleation is complete for  $m = 3$ , in consistency with the equilibrium analysis obtained before for  $M = 10$ . A peptide configuration at a nucleation event is shown on Fig. 8d indicating that a possible nucleus is a three-stranded  $\beta$ -sheet formed by three peptides (Fig. 8e). Fig. 8c shows that the system can form multiple aggregates of various sizes. The distribution of the aggregate size obtained after a sufficient long time is bimodal reflecting the fact that the system size is finite and clusters of less than 4 peptides are unstable. Thus, one either observes one large cluster with size close to the system size or several smaller clusters. The largest aggregates of  $m = 20$  peptides have the form of an elongated double  $\beta$ -sheet strongly resemble a cross- $\beta$ -structure (Fig. 8f).

Consider now the number of peptides in  $\beta$ -sheet conformation,  $n_\beta$ , which counts all the peptides that have at least 4 consecutive hydrogen bonds with another peptide. Fig. 9 shows the dependence of  $n_\beta$  on time  $t$ , with  $t$  measured in number of MC steps, averaged over the trajectories, for two different temperatures and for various concentrations. It is shown in Fig. 9 (a and b)

that for  $T = 0.2\epsilon/k_B$ , the time dependence of  $\langle n_\beta \rangle$  can be fitted well to the exponential relaxation function of  $M(1 - e^{-t/t_0})$ , where  $t_0$  is the characteristic time of aggregation. This time dependence also depends strongly on the concentration  $c$  with  $t_0$  increases more than 3 times by changing  $c$  from  $1$  mM to  $0.5$  mM. There seems to be no evidence of a lag phase at  $T = 0.2\epsilon/k_B$  as  $\langle n_\beta \rangle$  increases linearly with  $t$  for small  $t$  (Fig. 9b). This lack of evidence, however, may be due to the fact that the deviation from the exponential growth is too small to be observed. Indeed, we find that if the temperature is increased a little to  $T = 0.21\epsilon/k_B$ , the lag phase can be observed. Fig. 9c shows that the growth of  $\langle n_\beta \rangle$  in time is significantly deviated from the exponential relaxation function at small time. This growth when plotted in a log-log scale (Fig. 9c) shows that at small time  $\langle n_\beta \rangle \propto t^\alpha$  with  $\alpha \approx 1.25$ . The exponent  $\alpha > 1$  indicates that the time dependence of  $\langle n_\beta \rangle$  behaves like a convex function, which proves the existence of the lag phase at small time. The stronger evidence of the lag phase at  $T = 0.21\epsilon/k_B$  compared to that at  $T = 0.2\epsilon/k_B$  is consistent with the higher free energy barrier for nucleation at the former temperature previously shown in Fig. 7. Note that the lag phase has been also observed in the aggregation of homopolymers with a similar model but for a larger system<sup>31</sup>.

With the limited system size and time scale considered,

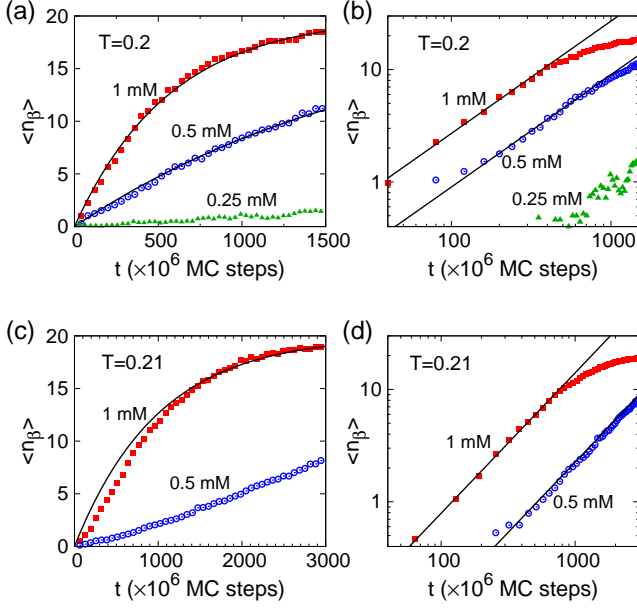


FIG. 9. Time dependence of the average number of peptides in  $\beta$ -sheet conformation,  $\langle n_\beta \rangle$ , in the aggregation of sequence S2 with  $M = 20$ . The system is considered at temperatures  $T = 0.2\epsilon/k_B$  (a,b) and  $0.21\epsilon/k_B$  (c,d) and at several concentrations,  $c = 1$  mM (squares),  $0.5$  mM (circles) and  $0.25$  mM (triangles), as indicated. The average of  $n_\beta$  for each concentration is taken over 100 independent trajectories. Right figures (b and d) plot the same data as in the left figures (a and c), respectively, except that in log-log scale. Data points are fitted to an exponential relaxation function of  $M(1 - e^{-t/t_0})$  for  $c = 1$  mM (solid) with  $t_0 = 570 \times 10^6$  for  $c = 1$  mM in (a) and  $t_0 = 1850 \times 10^6$  for  $c = 0.5$  mM in (a), and  $t_0 = 10^9$  for  $c = 1$  mM in (c). The log-log plots shows that the growth of  $n_\beta$  at small times follows a power law,  $\langle n_\beta \rangle \propto t^\alpha$ , with  $\alpha = 1$  in (b) and  $\alpha = 1.25$  in (d) for both concentrations of  $1$  mM and  $0.5$  mM.

we have not observed fragmentation of the fibril-like aggregates. On the other hand, the surface-catalyzed nucleation may exist from perspective of a two-layer  $\beta$ -sheet structure. The exposed hydrophobic side chains of the nucleated three-stranded  $\beta$ -sheet promotes association of other peptides by hydrophobic attraction. We find that clusters of 4 to 6 peptides often transform into a double  $\beta$ -sheet structure before continuing to grow. Thus, this secondary nucleation is surface-catalyzed and follows immediately after the primary nucleation event. The secondary nucleation also helps to stabilize the primary nucleus.

#### D. Aggregation of mixed sequences

Finally, we study the aggregation for a binary mixture of two sequences, S2 and S4. It was shown that in homogeneous systems, the first sequence is strongly fibril-prone, whereas the second one forms only  $\alpha$ -helices. Fur-

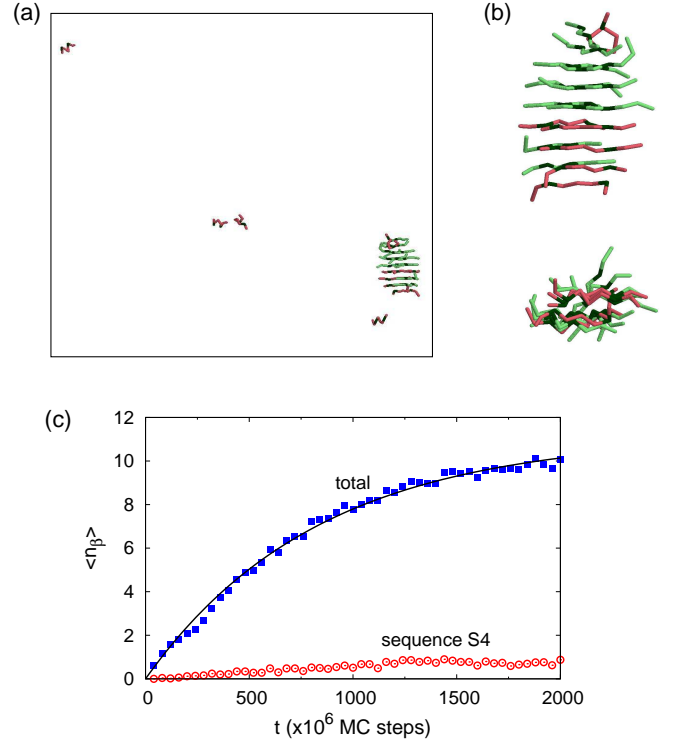


FIG. 10. (a) Snapshot of a conformation obtained in a simulation of the binary mixture of 10 chains of sequence S2 and 10 chains of sequence S4 at concentration  $c = 1$  mM and temperature  $T = 0.2\epsilon/k_B$ . H residues are shown in dark green. P residues are in light green and pink colors for the S2 and S4 chains, respectively. (b) Zoom-in side and top views of the aggregate shown in a. Note that six S4 chains are present in the aggregate, and five of them are in the  $\beta$ -sheet configuration. (c) Time dependence of the average number of peptides in  $\beta$ -sheet conformation,  $\langle n_\beta \rangle$ , obtained from 100 independent simulations, for both sequences together (squares) and for sequences S4 only (circles). A fit to the exponential relaxation function as given in the caption of Fig. 9 with  $t_0 = 832 \times 10^6$  (solid line) is shown for the case of both sequences.

thermore, the sequence S4 has the aggregation transition temperature lower than  $T^*$ , so the its aggregate is not stable at  $T^*$ . Strikingly, our simulations at  $T^*$  show that in a binary system of equally 10 chains of each sequence, after a sufficiently long time, a fraction of the S4 chains aggregate and convert into  $\beta$ -sheet conformation on an existing aggregate formed by the S2 chains (see Fig. 10). Though this fraction is only about 10% on average, this observation shows that the template-based mechanism for fibril formation can be effective for polypeptides of very different natures. Here, the fibril-like aggregate formed by the aggregation-prone peptides acts as the template for the aggregation of non-aggregation-prone peptides. Note that due to the mismatch of different hydrophobic patterns in the two sequences, the aggregates formed by the two sequences are more disordered than the homogeneous ones (Fig. 10b). It is also shown in Fig. 10c that the



growth of this mixed aggregate at the given temperature remains exponential but the characteristic time for aggregation is larger than in corresponding homogeneous system of sequence S2.

#### IV. DISCUSSION

Previous study of the tube model<sup>30</sup> has shown that hydrophobic-polar sequence can select protein's secondary and tertiary structures. In particular, the HPPH and HPPPH patterns have been identified as strong  $\alpha$ -formers, whereas the HPH pattern is a  $\beta$ -former. Strikingly, exactly the same binary patterns have been used in experiments that allow the successful design of de novo proteins<sup>46,47</sup>. In the present study, we find that these simple selection rules still hold for the peptides in aggregates, even though the model has been changed by considering the orientations of side chains. The present study shows that the binary pattern also determines the orderliness of the aggregate. In particular, there should be some compatibility between the alignment of hydrophobic side chains and the overall symmetry of the aggregate. Interestingly, the HPH pattern appears to be both a strong  $\beta$ -former and a highly aggregation-prone sequence. Our finding is in a full agreement with experimental design of amyloids<sup>15</sup>, which shows that segments of alternating hydrophobic and polar pattern (such as PHPHPHP) can direct protein sequences to form amyloid-like fibrils. This pattern has been also reported in a recent study of fibril formation using a lattice model<sup>48</sup>. Interesting, it has been also found that Nature disfavors this pattern in natural proteins<sup>15</sup>.

The important role of side chains in amyloid formation has been stressed in all-atom simulations<sup>22,44,49</sup>. In the tube model without considering the side chain orientations it was also possible to obtain amyloid-like aggregates<sup>29-32</sup>. These aggregates, however, are somewhat disordered in terms of  $\beta$ -sheet packing. Here, it is shown that with the side chain orientations the interaction between  $\beta$ -sheets can be directional leading to more ordered structures. This was shown for the sequences with alternating hydrophobic polar pattern whose hydrophobic side chains are oriented on one side of a  $\beta$ -sheet. The side chain directionality has been considered in a lattice model<sup>48</sup> leading to a similar result as in our present study. Note that other side chain features, such as size, shape and other specificities, should play some role as one increases the level of detail. For example, it has been shown that the excluded volume of side chain enhances the formation of helices and planar sheets<sup>36,50</sup>, which should be applied for the amyloid case as well. The hydrophobic contact potential with side chain orientations proposed in the present study can be considered as a first-order approximation accounting for the anisotropy of the interaction induced by the side chains.

Our thermodynamics results show that the formation of fibril-like aggregates is highly cooperative as indicated

by the height of the specific heat peak. This high cooperativity can be understood as due to the highly ordered nature of amyloid fibril structures and the dominating contribution of intermolecular interactions in these structures including hydrogen bonds and hydrophobic interaction. We also find that thermodynamic stability is not a distinguished feature of fibril-like aggregates. In particular, sequences with very high aggregation transition temperature do not necessarily form fibril-like aggregates. Our study shows that the HP pattern is a determinant of both amyloid characteristics of the aggregate and its thermodynamic stability, rather than the overall hydrophobicity of the sequence.

Our results on the kinetics of fibril formation show accordance to the current understanding of the mechanism of amyloid formation in terms of the nucleation process and the template-based growth, even though they may suffer from limited system size. It is interesting to note that the non-equilibrium kinetic behavior of a larger system is found to be consistent with equilibrium properties of smaller systems, given that the peptide concentration is constant. The small size of the initial nucleus found in the present study agrees with other coarse-grained<sup>31,32</sup> and all-atom simulation<sup>44</sup> studies. Our study indicates that the nucleus size depends on the choice of physiological temperature, or in other words the interaction strength in the system.

In a recent experiment, Ridgley *et al.*<sup>51</sup> show that mixtures of aggregation-prone peptides and proteins, including the rich in  $\alpha$ -helices myoglobin, self-assemble into amyloid fibers with increased amounts of cross- $\beta$  content. It was suggested that the  $\beta$ -sheet template formed by the peptides promotes the  $\alpha$  to  $\beta$  conversion in the proteins and their involvement in the cross- $\beta$  structure. Our simulation result on the peptide binary mixture is fully consistent with this experiment and shows that a cross- $\beta$ -sheet can be heterogeneous in its peptide composition. It is possible that naturally occurring amyloid fibrils can possess this heterogeneity due to the templated self-assembly process. A certain degree of heterogeneity can be seen in the fibril structure of HET-s prion protein<sup>10</sup>, which shows that the cross- $\beta$ -sheets are formed by repeating 'in-register' protein segments but neighboring  $\beta$ -strands do not have the same amino acid sequence.

#### V. CONCLUSION

The present study has highlighted several aspects of amyloid fibril formation that include the sequence determination of fibrillar structures, the role of side chain directionality, the thermodynamics of aggregation, and the nucleation and template-based growth mechanism. In agreement with various experimental findings, our results indicate that fibril-like aggregates form very much under the same principles as in protein folding, such as the alignment of hydrophobic residues in a  $\beta$ -sheet, the packing of hydrophobic side chains, and the cooperativity

of the aggregation transition. These principles are mainly associated to the specificity of a sequence. Our simulations also show another feature of amyloid formation, that is considerably non-specific to a sequence, namely the fibril-induced aggregation of a non-aggregation-prone sequence. This templating property certainly complicates the problem of amyloid formation as it suggests that the cross- $\beta$ -structure can be heterogeneous in their sequence or peptide composition. Our study provides a basis for finding the routes to deal with the problem.

This research is funded by Vietnam National Foundation for Science and Technology Development (NAFOS-TED) under Grant No. 103.01-2016.61. The use of computer cluster at CIC-VAST is gratefully acknowledged.

- <sup>1</sup>F. Chiti and C. M. Dobson, *Annu. Rev. Biochem.* **75**, 333 (2006).
- <sup>2</sup>R. Riek and D. S. Eisenberg, *Nature (London)* **539**, 227 (2016).
- <sup>3</sup>J. L. Jimenez, J. I. Guijarro, E. Orlova, J. Zurdo, C. M. Dobson, M. Sunde, and H. R. Saibil, *EMBO* **18**, 815 (1999).
- <sup>4</sup>C. M. Dobson, *Trends Biochem. Sci.* **24**, 329 (1999).
- <sup>5</sup>M. Fändrich and C. M. Dobson, *EMBO* **21**, 5682 (2002).
- <sup>6</sup>S. Ventura, *Micro. Cel. Fact.* **4**, 11 (2005).
- <sup>7</sup>M. Sunde, L. C. Serpell, M. Bartlam, P. E. Fraser, M. B. Pepys, and C. C. Blake, *J. Mol. Biol.* **273**, 729 (1997).
- <sup>8</sup>J. L. Jiménez, E. J. Nettleton, M. Bouchard, C. V. Robinson, C. M. Dobson, and H. R. Saibil, *Proc. Natl. Acad. Sci. USA* **99**, 9196 (2002).
- <sup>9</sup>A. T. Petkova, Y. Ishii, J. J. Balbach, O. N. Antzutkin, R. D. Leapman, F. Delaglio, and R. Tycko, *Proc. Natl. Acad. Sci. USA* **99**, 16742 (2002).
- <sup>10</sup>C. Wasmer, A. Lange, H. Van Melckebeke, A. B. Siemer, R. Riek, and B. H. Meier, *Science* **319**, 1523 (2008).
- <sup>11</sup>M. D. Tuttle, G. Comellas, A. J. Nieuwkoop, D. J. Covell, D. A. Berthold, K. D. Kloepper, J. M. Courtney, J. K. Kim, A. M. Barclay, A. Kendall, *et al.*, *Nat. Struct. Mol. Biol.* **23**, 409 (2016).
- <sup>12</sup>M. R. Sawaya, S. Sambashivan, R. Nelson, M. I. Ivanova, S. A. Sievers, M. I. Apostol, M. J. Thompson, M. Balbirnie, J. J. Wiltzius, H. T. McFarlane, *et al.*, *Nature (London)* **447**, 453 (2007).
- <sup>13</sup>A. T. Petkova, R. D. Leapman, Z. Guo, W.-M. Yau, M. P. Mattson, and R. Tycko, *Science* **307**, 262 (2005).
- <sup>14</sup>B. H. Meier and A. Böckmann, *Curr. Opin. Struct. Biol.* **30**, 43 (2015).
- <sup>15</sup>M. W. West, W. Wang, J. Patterson, J. D. Mancias, J. R. Beasley, and M. H. Hecht, *Proc. Natl. Acad. Sci. USA* **96**, 11211 (1999).
- <sup>16</sup>C. Wurth, N. K. Guimard, and M. H. Hecht, *J. Mol. Biol.* **319**, 1279 (2002).
- <sup>17</sup>F. Chiti, N. Taddei, F. Baroni, C. Capanni, M. Stefani, G. Ramponi, and C. M. Dobson, *Nat. Struct. Mol. Biol.* **9**, 137 (2002).
- <sup>18</sup>S. Ventura, J. Zurdo, S. Narayanan, M. Parreño, R. Mangues, B. Reif, F. Chiti, E. Giannoni, C. M. Dobson, F. X. Aviles, *et al.*, *Proc. Natl. Acad. Sci. USA* **101**, 7258 (2004).
- <sup>19</sup>M. L. de la Paz, K. Goldie, J. Zurdo, E. Lacroix, C. M. Dobson, A. Hoenger, and L. Serrano, *Proc. Natl. Acad. Sci. USA* **99**, 16052 (2002).
- <sup>20</sup>M. L. de la Paz and L. Serrano, *Proc. Natl. Acad. Sci. USA* **101**, 87 (2004).
- <sup>21</sup>S. Alberti, R. Halfmann, O. King, A. Kapila, and S. Lindquist, *Cell* **137**, 146 (2009).
- <sup>22</sup>M. L. de la Paz, G. M. de Mori, L. Serrano, and G. Colombo, *J. Mol. Biol.* **349**, 583 (2005).
- <sup>23</sup>M. S. Li, G. Reddy, C.-K. Hu, J. Straub, D. Thirumalai, *et al.*, *Phys. Rev. Lett.* **105**, 218101 (2010).
- <sup>24</sup>A.-M. Fernandez-Escamilla, F. Rousseau, J. Schymkowitz, and L. Serrano, *Nat. Biotech.* **22**, 1302 (2004).
- <sup>25</sup>A. Trovato, F. Seno, and S. C. Tosatto, *Protein Eng. Des. Sel.* **20**, 521 (2007).
- <sup>26</sup>S. Maurer-Stroh, M. Debulpaepe, N. Kuemmerer, M. L. De La Paz, I. C. Martins, J. Reumers, K. L. Morris, A. Copland, L. Serpell, L. Serrano, *et al.*, *Nat. Meth.* **7**, 237 (2010).
- <sup>27</sup>T. X. Hoang, A. Trovato, F. Seno, J. R. Banavar, and A. Maritan, *Proc. Natl. Acad. Sci. USA* **101**, 7960 (2004).
- <sup>28</sup>A. Maritan, C. Micheletti, A. Trovato, and J. R. Banavar, *Nature (London)* **406**, 287 (2000).
- <sup>29</sup>J. R. Banavar, T. X. Hoang, A. Maritan, F. Seno, and A. Trovato, *Physical Review E* **70**, 041905 (2004).
- <sup>30</sup>T. X. Hoang, L. Marsella, A. Trovato, F. Seno, J. R. Banavar, and A. Maritan, *Proc. Natl. Acad. Sci. USA* **103**, 6883 (2006).
- <sup>31</sup>S. Auer, C. M. Dobson, and M. Vendruscolo, *HFSP journal* **1**, 137 (2007).
- <sup>32</sup>S. Auer, C. M. Dobson, M. Vendruscolo, and A. Maritan, *Phys. Rev. Lett.* **101**, 258101 (2008).
- <sup>33</sup>K. A. Dill and H. S. Chan, *Nat. Struct. Biol.* **4**, 10 (1997).
- <sup>34</sup>O. Gonzalez and J. H. Maddocks, *Proc. Natl. Acad. Sci. USA* **96**, 4769 (1999).
- <sup>35</sup>N. B. Hung and T. X. Hoang, in *Journal of Physics: Conference Series*, Vol. 627 (IOP Publishing, 2015) p. 012028.
- <sup>36</sup>J. R. Banavar, M. Cieplak, T. X. Hoang, and A. Maritan, *Proc. Natl. Acad. Sci. USA* **106**, 6900 (2009).
- <sup>37</sup>R. H. Swendsen and J.-S. Wang, *Phys. Rev. Lett.* **57**, 2607 (1986).
- <sup>38</sup>A. M. Ferrenberg and R. H. Swendsen, *Phys. Rev. Lett.* **63**, 1195 (1989).
- <sup>39</sup>J. Hanson and J. Lowy, *J. Mol. Biol.* **6**, 46 (1963).
- <sup>40</sup>F. Oosawa and M. Kasai, *J. Mol. Biol.* **4**, 10 (1962).
- <sup>41</sup>W.-F. Xue, S. W. Homans, and S. E. Radford, *Proc. Natl. Acad. Sci. USA* **105**, 8926 (2008).
- <sup>42</sup>E. Hellstrand, B. Boland, D. M. Walsh, and S. Linse, *ACS Chem. Neurosci.* **1**, 13 (2009).
- <sup>43</sup>T. P. Knowles, C. A. Waudby, G. L. Devlin, S. I. Cohen, A. Aguzzi, M. Vendruscolo, E. M. Terentjev, M. E. Welland, and C. M. Dobson, *Science* **326**, 1533 (2009).
- <sup>44</sup>P. H. Nguyen, M. S. Li, G. Stock, J. E. Straub, and D. Thirumalai, *Proc. Natl. Acad. Sci. USA* **104**, 111 (2007).
- <sup>45</sup>A. M. Ruschak and A. D. Miranker, *Proc. Natl. Acad. Sci. USA* **104**, 12341 (2007).
- <sup>46</sup>S. Kamtekar, J. M. Schiffer, H. Xiong, J. M. Babik, and M. H. Hecht, *Science* **262**, 1680 (1993).
- <sup>47</sup>Y. Wei, S. Kim, D. Fela, J. Baum, and M. H. Hecht, *Proc. Natl. Acad. Sci. USA* **100**, 13270 (2003).
- <sup>48</sup>S. Abeln, M. Vendruscolo, C. M. Dobson, and D. Frenkel, *PLoS One* **9**, e85185 (2014).
- <sup>49</sup>J. Gsponer, U. Haberthür, and A. Caflisch, *Proc. Natl. Acad. Sci. USA* **100**, 5154 (2003).
- <sup>50</sup>T. Škrbić, T. X. Hoang, and A. Giacometti, *J. Chem. Phys.* **145**, 084904 (2016).
- <sup>51</sup>D. M. Ridgley, K. C. Ebanks, and J. R. Barone, *Biomacromolecules* **12**, 3770 (2011).